ALTERATION OF CHROMATIN STRUCTURE DURING LPS TOLERANCE ACQUISITION IN *Salmonella enterica*-INFECTED MACROPHAGES

A PREPRINT

Cyril Matthey-Doret[1,2], Peter W. Hill[3], Agnès Thierry[1], Sophie Helaine[4,*], Romain Koszul[1,*]

October 18, 2021

1 Institut Pasteur, Spatial Regulation of Genomes unit, CNRS, UMR 3525, C3BI USR 3756, Paris, France
2 Sorbonne Université, Collège Doctoral, F-75005 Paris, France
3 Department of Medicine, MRC CMBI, Imperial College London, London, UK
4 Department of Microbiology, Harvard Medical School, 77 Ave Pasteur, Boston, MA 02115, USAHMS Department of Microbiology, Harvard, US

ABSTRACT

In vertebrates, the immune response to bacterial infection involves a complex balance to clear infectious agents without damaging the tissues. During prolonged infections, LPS tolerance is key to this balance, causing a temporary reduction in the inflammatory response to regenerate and preserve tissues. Many regulatory layers are important to coordinate infectious response, including phosphorylation cascades, histone modifications, and micro-RNAs. Gene expression and epigenetic changes are often intertwined with spatial organization of the genome. In this work, we study changes in chromatin structure during infection of murine bone macrophages by *Salmonella enterica*. We find global changes during late infection, when LPS tolerance is thought to take place and identify several pathways associated with chromatin changes.

***K*eywords** Genomics · Hi-C · Host-parasite · Infection

Introduction

Salmonella is an intracellular bacterium and human pathogen causing an enteric disease known as salmonellosis in many animals. It is usually contracted by ingestion of contaminated foods or water and infiltrates the intestinal epithelium. Salmonella destabilizes tight junctions between epithelial cells, favoring the migration of neutrophils through the epithelial layer by stimulating the mitogen-activated protein kinase (MAPK) and NF-κB pathways [1, 2]. The sensing of bacterial lipopolysaccharides (LPS) present on the bacterial cell surface by immune cells through Toll-like receptors (TLR) elicits the production of interleukins and activation of caspase genes [3], which further increases intestinal inflammation.

Salmonella cellular infection is mediated by two type 3 secretion systems (T3SS), encoded by distinct pathogenicity islands, *Salmonella pathogenicity island* (SPI) 1 and 2. Both T3SS mediate the transfer of bacterial proteins (or effectors) into the host-cell cytoplasm, but they are active at different time during infection. The SPI1 T3SS is used mainly for invasion of non-phagocytic cells and induction of inflammatory response, whereas the SPI2 T3SS is important for bacterial survival in macrophages and establishment of systemic disease [4].

Salmonella can infect many cell types in the epithelium by T3SS SPI1-mediated endocytosis, and enter macrophages through phagocytosis [5]. During systemic infection, macrophages phagocytose *Salmonella* at mesentric lymph nodes and transport the bacteria to other sites such as the spleen, liver and bone marrow [6]. The bacterium can survive

for long periods in these macrophages and form ganulomas. Upon cell entry, Salmonella secretes effector proteins through its T3SS to manipulate the host defenses and metabolism, and replicate inside the cell. A combination of replicating and non-replicating bacteria can co-exist within the host cell [7]. Non-replicating cells - also called persisters - have increased antibiotic recalcitrance and are of particular concern for the relapse of *Salmonella* infection following stoppage of antibiotic treatment [8].

In response to bacterial infection, host macrophages secrete chemokines and cytokines to recruit other immune cells to the infection site. They also produce reactive oxygen species (ROS) and microbicidal molecules to kill surrounding bacterial cells [9, 10]. This response is stimulated by LPS present on the cell surface of gram-negative bacteria such as *Salmonella*. However, in cases of intense and prolonged exposure, this can lead to over-stimulation of the immune system, sometimes resulting in an endotoxic shock which poses the threat of tissue damage, organ failure and death. To avoid such outcome, the body can enter a transient state of hyporesponsiveness to infection known as endotoxin-tolerance, or LPS-tolerance. During this period, macrophages are reprogrammed to cease production of inflammatory molecules and instead focus on tasks such as tissue repair and phagocytosis of cellular debris [11].

A complex interplay takes place between host inflammatory factors and bacterial effectors. Upon invasion of the intestinal lumen by *Salmonella*, the release of ROS by macrophages leads to a growth advantage for the pathogen over resident bacteria from the microbiome [12]. Conversely, after cellular entry, *Salmonella* effectors dampen inflammation to favor intracellular survival, reducing IL-8 secretion and MAPK-mediated inflammation using its effector proteins [13]. This suggests that *Salmonella* can increase or decrease inflammatory response depending on the stage of infection. Understanding how bacteria manipulate the host immune response is an important step towards treating and mitigating risks associated with *Salmonella* infection. Many levels or regulation are affected by the bacterium, including signal transduction pathways [14], mitochondrial metabolism [15], RNA splicing [16] and histone marks [17].

In mammals, gene regulation is intertwined with genome compaction and folding. At the broadest level, chromatin is segregated into active and inactive compartments, which can change according to the needs of the cell [18]. The genome is also partitioned into Topologically Associating Domains (TADs) which can form insulated neighbourhood genes and regulatory elements [19]. Regulatory interactions are also mediated by chromatin loops which can modulate gene activity by putting them in physical contact with enhancers or promoters. In mammals, these chromatin structures are mainly orchestrated by the CCTC-binding factor (CTCF) [20]. CTCF-mediated loops are thought to play roles in immunity, such as increasing the expression of genes in the major histocompatibility complex (MHC) locus [21, 22, 23], or coordinating the expression of interleukins [24, 25]. The LPS-tolerance phenomenon is thought to be regulated by epigenetic mechanisms such as histone modifications [26, 27, 28], but thus far there has been little investigation of the implication of genome conformation in that process.

Here we investigate the consequences of *Salmonella* infection on the genome structure of mammalian host cells. Using Hi-C in Mouse bone marrow macrophages (BMM), we measure spatial genomic features at early and late Salmonella infection and how they relate to gene deregulation. We find genome-wide changes in chromatin compartments and overall organization during late infection (around 20h post infection). This coincides with the time at which LPS tolerance is acquired [29]. We find large compartment switches associated with the MHC complex and chemokine genes. We also identify strong changes in chromatin loops, compartment and expression associated with chemokine genes, known to regulate cell migration and chemotaxis. Finally, we observe changes in expression and long range interactions during infection for several markers of LPS tolerance, as well as the anti-inflammatory cytokine Interleukin-10.

Results

Chromosome folding is altered in late infection

We used Hi-C to capture chromosome conformation of murine BMM infected by *Salmonella* as well as bystander cells exposed to *Salmonella*. Hi-C was performed in uninfected cells and at two time points representing early (2h) and late (20h) infection. We also a ΔSsaV mutant *Salmonella*, deficient for the T3SS SPI2 and unable to inject effector proteins into the host cytoplasm. We used 3 different Hi-C derived features to measure chromosome structural changes: The stratum-adjusted correlation coefficient [30], which measures overall contact similarity between Hi-C matrices of sample pairs (Fig. 1a), the slope of the distance-contacts decay function (Fig. 1b), which reflects chromatin compaction averaged over the genome, and A/B compartment eigenvectors (Fig. 1c), which encode the segmentation of the genome into active and inactive chromatin. We found that most changes happened during late (20h) infection, regardless of *Salmonella* genotype or bystander versus infected status. Infection time point (20h vs 2h) was the main determinant with respect to all 3 aforementioned features.

The time at which we observe strongest conformational changes coincides with the time range for the acquisition of LPS tolerance (16 - 48h) [31]. To focus on such changes, we re-sequenced Hi-C libraries from samples infected by

WT Salmonella at those time points (each time point in duplicates). This allowed us to inspect changes in fine grained chromatin structures, such as chromatin loops and TAD borders.

We used Hi-C to measure compartment changes at two time points in infected cells. Genome-wide A/B compartmentalization was more pronounced at late infection (Fig. 1d) compared to early infection or uninfected cells. These large scale changes could be attributed to physiological changes in late infection.

When investigating the expression of known LPS-response marker genes described in [29], we found negative regulators of the LPS response to be upregulated in late infection (Fig. S1a), with some of them undergoing changes in chromatin loops (Fig. S1b). We also find the groups of previously reported positive and negative regulators of LPS-tolerance to be largely consistent with our differential expression results (Fig. S1c)

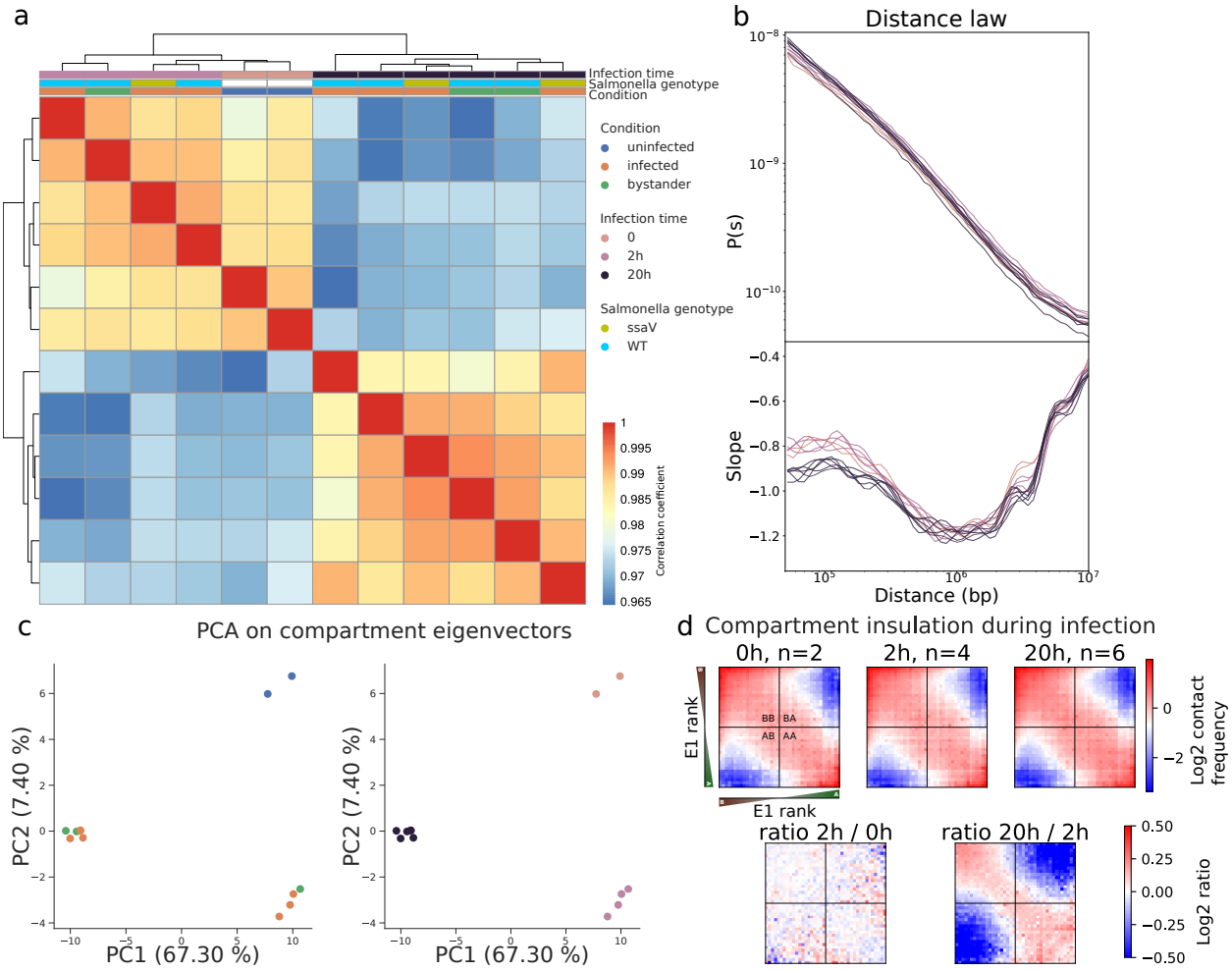

Figure 1: Global changes in genome conformation happen during late Salmonella infection. **a,** Heatmap of HiCRep stratum adjusted correlation coefficients between all pairs of samples. **b,** Distance-dependent contact decay (top) and its slope (bottom) according to infection time. **c,** PCA of chromatin compartment vectors with samples colored by condition (top) and infection time (bottom). **d,** Saddle plots showing compartment insulation intensity during infection. Hi-C interactions are binned according to their rank on the compartment eigenvector (E1) and discretized into quantiles. Saddle plots show the average intensity of interactions between each pair of eigenvector quantile (top) and their change during infection (bottom) using the Log ratio of saddles between different time points.

Global structural changes in the MHC region

We used CHESS [32] to detect non-specific structural changes occuring between early and late infection. CHESS extracted 350 features corresponding to structural changes, encompassing a total of 1110 genes. We performed a functional enrichment analysis using Gprofiler [33] to identify gene ontology terms enriched in structural changes.

Among all 155 significant terms (full list in table S1), the most strongly enriched terms are related to antigen presentation and the Major Histocompatibility Complex (MHC) (Fig. 2a). A visible compartment change is observed in the magnified contact map of the corresponding region, (Fig. 2b) as well as an insulation change, at a finer resolution. Out of the 7 MHC genes located in the region identified by CHESS (H2-Q1,2,4,6,7,10 and H2-D1), 3 have significantly higher expression during late infection (H2-Q4,6,7, log fold changes 0.6, 1.9 and 1.9).

Chromatin alterations are enriched in cell migration pathways

We ran gene set enrichment analysis (GSEA) separately on 4 differential features during late infection (20h vs 2h): A/B compartment, chromatin loops, domain borders and gene expression. After multiple testing correction (Benjamini Hochberg, FDR rate=0.1), all 4 features are enriched in gene sets related to leukocyte chemotaxis and migration. To visually explore the relationship between structural features and expression, and the gene set overlap between GO terms, we generated a graph from all gene sets with (non-corrected) p-values below 0.05 using Enrichment Map [34] (methods). In this graph, each node represents the gene set of a GO term, and nodes are connected if they share at least 37.5% of their genes. Nodes are colored according to the features in which they were found to have a significant p-values. The largest connected component of this graph contains GO terms related to chemotaxis and migration, as well as other pathways (Fig. 3a). Chromatin features are limited to certain modules of that graph, while gene expression is deregulated in most nodes.

The genes associated with structural and expression changes in sets pertaining to chemotaxis mostly belong to a cluster of chemokine ligand (CXCL) genes (Fig. 3b). These genes produce small cytokines controlling the migration and adhesion of monocytes and have previously been associated with increased expression in LPS tolerance [27]. In addition, CXCL5 and CXCL9 expression is thought to be maintained through histone acetylation and methylation [27]. Our results suggest that these histone modifications could be accompanied by changes in chromatin loops and borders, as well as a global switch to the A compartment (Fig. 3b).

Increase in chromatin looping at the IL-10 locus

The position of chromatin loops anchors were refined using ATAC-seq peaks and classified based on their location (TSS, TTS, inter-gene, intronic, exonic). This classification was further expanded using publicly available ChIP-seq datasets of histone marks in BMM to include enhancer, promoter and repressed (Methods, S2). Among loops overlapping differential ATAC-seq peaks (20h vs 2h p.i), we found 36 loops anchored at the promoters of differentially expressed genes, including genes related to cell adhesion and cytoskeleton (ACTN1, ICAM5, P2RX4, TGFB1).

We also found a chromatin loops appearing next to the Il-10 gene and forming contacts with the Fcmr and Il-24 genes, both of which harbour repressive marks and did not have detectable expression in our RNA-seq data. The anti-inflammatory cytokin interleukin 10 (IL-10) downregulates the inflammatory response to prevent damage to the host. Its expression is regulated by CTCF [24], and it is thought that chromatin looping coordinates the gene expression in that locus [24]. We found an increase in chromatin loop strength during late infection, further supporting the role of CTCF looping in interleukin regulation.

Il-10 is activated by the TLR4 pathway which directly depends on LPS stimulation. While its expression upon LPS stimulation is known to be stronger in tolerized macrophages compared to naive macrophages, we found a lower expression of IL-10 in late infection compared to early infection (log2 fold change: -4.55, q-value: 4e-147). This is likely due to the absence of LPS-restimulation in late infection.

Discussion

In this work, we studied changes in chromatin organization of muring BMM following infection by *Salmonella enterica*. We found that most changes in global chromatin structure happened at late infection (20h p.i.), whereas it is mostly unchanged in early (2h p.i.) infection. This time point corresponds with the onset of LPS tolerance, which was shown to be dependant on histone modifications [27]. While response to acute infection is accompanied by extensive changes in local chromatin accessibility [35], we found no substantial changes in 3D chromatin reorganisation. These results are largely in keeping with the proposed role of regulators of 3D chromatin structure (i.e., Cohesin, CTCF) organising the macrophage genome in a way that facilitates rapid response to TLR signalling [24, 36].

We observed an enrichment of chromatin structural changes, and general upregulation of genes involved in chemotaxis and cell migration during late infection. Interestingly, it was shown that M2 macrophages, which share other key characteristics with the macrophage phenotype associated with LPS tolerance, are more motile [37].

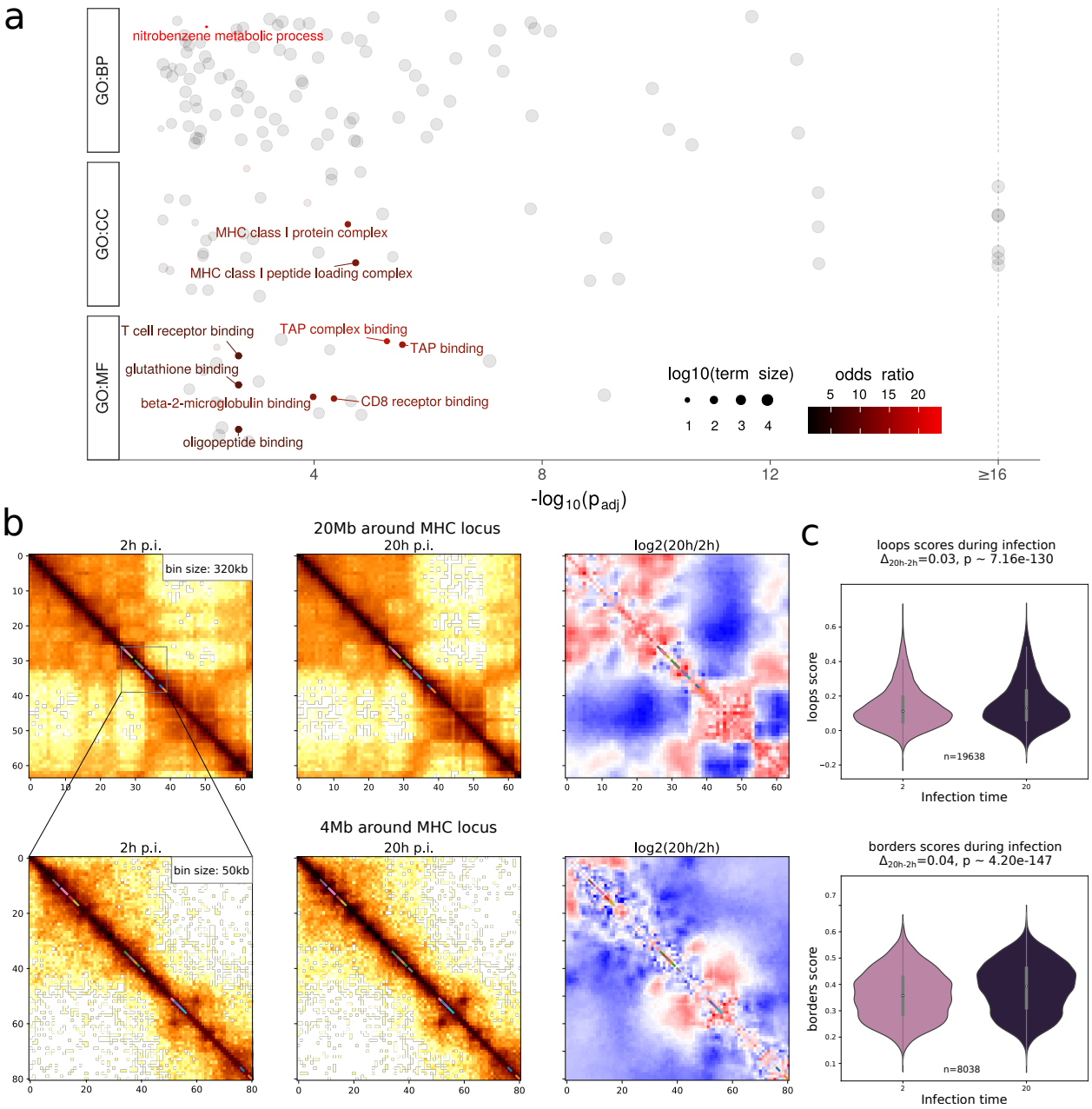

Figure 2: Hi-C changes during late infection. **a,** Overrepresentation analysis analysis of gene ontology terms in CHESS-positive regions showing structural changes during infection. The top 10 terms with highest enrichment odds ratio are highlighted. Point size represent the number of genes constituting a GO term, and the horizontal position represents the p-value from Fisher exact test adjusted for multiple testing using g:profiler's SCS algorithm [33]. Terms are split into 3 based on their GO category: CC (cellular component), BP (biological process) or MF (molecular function). **b,** Hi-C contacts around the MHC locus at low (top) and medium (bottom) resolutions. Contacts are shown during early (left) and late (middle) infection. The serpentine-binned ratio showing contact changes during infection is shown on the right. Colored lines on the main diagonal represent MHC genes identified by CHESS as part of a structural change. **c,** Distribution of loops (top) and borders (bottom) intensity throughout the whole genome at early and late infection. Pileup plots show the average 2D profile of patterns in each condition. P-values are computed using Wilcoxon's signed-rank test.

The large compartment switch we observe at the MHC locus, along with increased expression of several H2-Q genes are consistent with previous findings based on microscopy observations that transcriptional changes at the MHC locus are associated with chromatin reorganization [38], however the role of H2-Q family genes is still poorly understood [39].

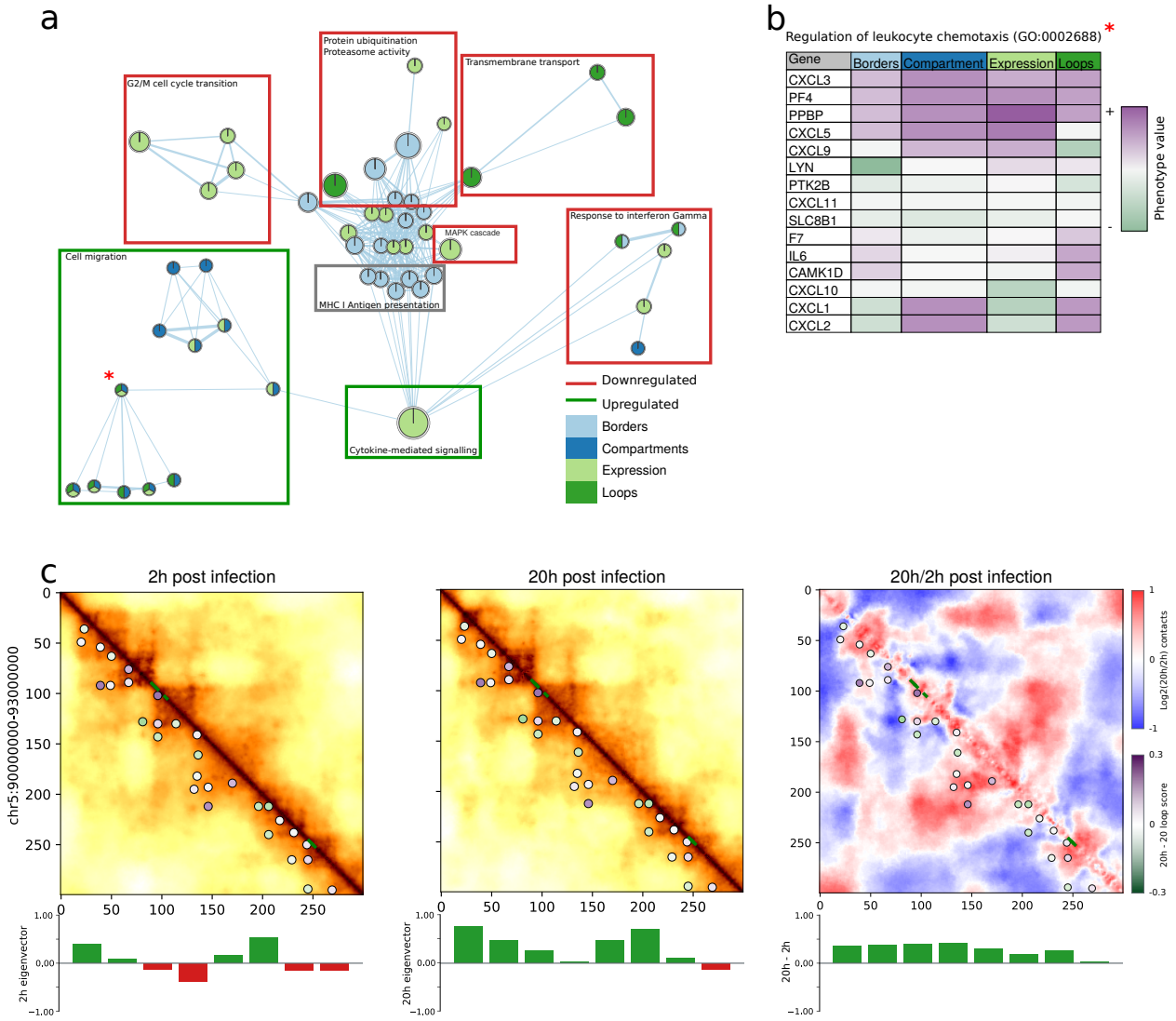

Figure 3: Gene set enrichment analysis of chromatin features. **a,** Largest connected component of the GSEA graph from chromatin features and gene expression change in . Each node is a GO:BP term, edges represent the proportion of gene overlap between terms (minimum cutoff 37.5%). Nodes are colored according to the feature (expression, compartment, border or loop change) in which they are significantly enriched during late infection (20h vs 2h). Functional subregions of the graph have been manually annotated, and the frame is colored based on its gene expression change (red: significantly downregulated, green: significantly upregulated, grey: neutral). **b,** Feature enrichment for genes involved in the GO term "Regulation of leukocyte chemotaxis", denoted by a red star on the graph. **c,** Hi-C contacts in the region containing chemokine genes CXCL3 and CXCL5. Chemokine genes are highlighted in green along the main diagonal. All matrices were binned at 10kb resolution and smoothed using Serpentine adaptive binning.

Similarly, the chromatin looping observed at Il-10 confirms previous observations. It is especially interesting that the inhibition of Il-10 expression is associated with specific interactions at genic regions harboring repressive marks. Unfortunately, further investigation would require histone ChIP-seq from infected macrophages which was not performed in this study, as histone marks used here are derived from resting BMM and may be markedly different from LPS-stimulated BMM.

Generally, the absence of chromatin changes during early infection could suggest that large structural changes operate on a slower time scale and are more adapted to the establishment of long term tolerance.

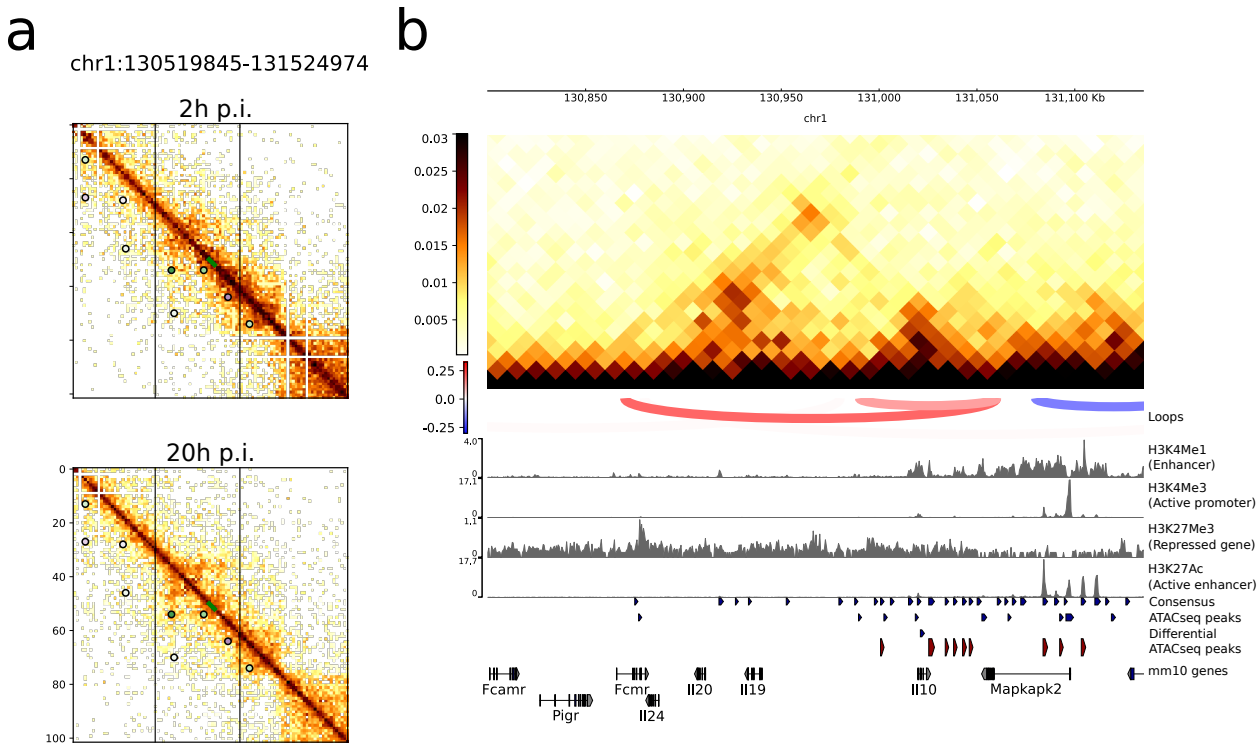

Figure 4: **a,** Contact map region in a 1Mbp region around the Il10 gene in early (2h) and late (20h) infection. Vertical black liines indicate the region shown in b. **b,** Epigenetic landscape around IL-10. A chromatin loop anchored next to the Il10 gene appears at 20h p.i. (top). The right anchor falls into a region with enhancer epigenetic marks. The left anchor falls close to Il24 and is rich in repressive marks.

Methods

Libraries preparation

Hi-C library preparation

Hi-C libraries were prepared according to the Arima protocol using only the DpnII and HinfI enzymes. Libraries were sequenced using paired end sequencing at 35bp on an Illumina NextSeq 500 machine.

ATAC-seq library preparation

ATAC-seq library preparation was carried out according to the published Omni-ATAC protocol [40]. Libraries were sequenced on an Illumina NextSeq 500 using paired end sequencing.

RNA-seq library preparation

RNA was isolated using the Quick DNA-RNA Miniprep Kit following the manufacturer's protocol. Following RNA isolation, macrophage rRNA was depleted using the NEBNext rRNA Depletion Kit following the manufacturer's protocol. RNA-Seq libraries were generated using the NEBNext Ultra II Directional RNA Library Kit for Illumina and the NEBNext Multiplex Oligos for Illumina following the manufacturer's protocol. Libraries were sequenced on an Illumina NextSeq 500 using single read sequencing.

RNA-Seq/ATAC-Seq infections and FACS sorting

Wild type or ΔssaV *Salmonella enterica* serovar Typhimurium (strain SL1344) expressing the pFCcGssaG plasmid (i.e. ssaG promoter expressed GFP, constitutive mCherry) [41] were grown overnight in MgMES pH 5.0 medium (170 mM 2-(N-morpholino)ethanesulfonic acid (MES) at pH 5.0, 5 mM KCl, 7.5 mM $(NH_4)_2SO_4$, 0.5 mM K_2SO_4,

1 mM KH_2PO_4, 8 mM $MgCl_2$, 38 mM glycerol, and 0.1% casamino acids). Stationary phase bacteria were then opsonized with 8% mouse serum for 20 minutes and added to the BMDM at a MOI of 10. At 30 min post-infection, macrophages were washed 3x with PBS, and fresh BMDM medium containing gentamicin (50 μg/ml) was added. At 2.5 h post-infection, macrophages were washed 1x with PBS, and fresh BMDM medium containing gentamicin (10 μg/ml) was added. Prior to isolation by FACS, uninfected macrophages and macrophages at 2h and 18h post-infection were washed with PBS three times and detached from the surface with cold PBS and scraping. Macrophages were then centrifuged at 4 °C at 300g, the supernatant discarded, and macrophages resuspended in cold sterile PBS. For infected macrophages, 5E4 macrophages containing either wild type or ΔssaV Salmonella (mCherry+ population) were isolated by FACS. For uninfected macrophages, 5E4 macrophages were isolated by FACS. For FACS isolation, apoptotic macrophages and doublets were excluded by gating, and the samples were sorted under continuous cooling to 4 °C by a BD Aria III into cold sterile PBS. Isolated macrophages in PBS were then centrifuged at 500g for 5 min at 4 °C, the supernatant was removed, and macrophage pellets were either used immediately for ATAC-seq library preparation or snap frozen in liquid nitrogen and stored at -80 °C until RNA was isolated for RNA-Seq library preparation.

Analyses

All analyses were done using the mm10 reference genome assembly.

Differential accessibility peaks

ATACseq data was processed using the nf-core/atacseq pipeline (v1.2.1). Within nfcore/atacseq, consensus peaks were obtained using MACS2 (v2.2.7.1) and differential peaks from DESeq2 with FDR<0.05 were selected.

Histone marks ChIPseq

Publicly available histone mark ChIPseq datasets were retrieved from ENCODE and processed using the nf-core/chipseq pipeline (v1.2.1) in single-end mode. The following marks and respective accession numbers were used: H3K4Me1 (ENCSR000CFE), H3K4Me2 (SRR930721, SRR930722), H3K4Me3 (ENCSR000CFF), H3K27Me3 (SRR930746), H3K27Ac (ENCSR000CFD).

Differential expression

Libraries were aligned using Hisat2 (1.24.0.123) and transcripts were quantified into TPM using salmon (v0.14.1). Differential expression was measured between 2h and 20h p.i. using DESeq2.

Hi-C analyses

Hi-C matrices were generated using hicstuff (v3.0.1) [42]. Matrix balancing (normalization) was performed using the Cooler implementation of the ICE algorithmm [43] Compartments were extracted using the cooltools API [44].

Reproducibility between replicates was assessed using the hicreppy implementation (`https://github.com/cmdoret/hicreppy`)of the HiCrep algorithm [30]. Briefly, a correlation coefficient is computed between pairs of sample for each diagonal separately, and a weighted average of correlation coefficients is then returned, with the weights being inversely proportional to the genomic distance corresponding to each diagonal. The operation is performed separately on each chromosome, and the average of all chromosomes, weighted by their length is used.

Chromatin loops and domain borders were detected using chromosight [45] (v1.5.1) and pattern intensity changes between conditions were computed using pareidolia (v.0.6.0) [46]. Compartment segmentation was performed using cooltools (v0.3.2) [44] using the correlation with gene density to orient eigenvectors. Hi-C matrices were binned at 320kb for compartment detection and Hi-C rep and 10kb for all other analyses.

Each gene was assigned the closest loop anchor and domain border within 200kb (if any). CHESS was used to identify genes located in regions undergoing major structural changes during infection.

Gene set enrichment analysis

GSEA was performed using the python package gseapy [47]. The analysis was run 4 times independently on different phenotypes representing changes between 2h and 20h p.i. The phenotypes used were: differential pattern scores (loop and borders) from Pareidolia, compartment eigenvector differences from cooltools, and gene expression log2 fold change from DeSeq2. For structural phenotypes, values were assigned to genes using bedtools genome arithmetic operations [48]: Borders and loops were assigned to the closest gene within 200kb, and compartment values were assigned to genes using bedtools intersect.

For visualizing the network graph, the union of all terms with p-values below 0.05 (without multiple testing correction) for all phenotypes was used. The graph was generated using cytoscape with the enrichmentMap plugin [34]. Nodes were colored by dataset (i.e. where the phenotypes' p-values are below 0.05) for visualization.

Integration of epigenomic data

Chromatin loops in figure S2 were intersected with differntial ATAC peaks to refine retain only loops with both anchors within 10kb (a margin of 1 pixel on the Hi-C contact map) of differentially accessible ATAC peaks (FDR <0.05). Average normalized histone mark intensity scores were assigned to each peak and K-means clustering (k=3) was used on those intensities to classify anchors into 3 groups: promoter (highest H3K4Me3), enhancer (highest H3K4Me1) or low activity (other peaks). Peaks were histone marks were not available were labelled "unknown". Promoter anchors were further refined to include only those located in promoter regions (-1kb to +100bp from TSS).

Code availability

All codes to reproduce analyses is available on a Github repository at `https://github.com/cmdoret/mouse_salmonella_infection.git` where data processing is packaged into a Snakemake pipeline, and downstream analyses are provided as jupyter notebooks.

References

[1] B A McCormick, S I Miller, D Carnes, and J L Madara. Transepithelial signaling to neutrophils by salmonellae: A novel virulence mechanism for gastroenteritis. *Infection and Immunity*, 63(6):2302–2309, June 1995.

[2] B A McCormick, P M Hofman, J Kim, D K Carnes, S I Miller, and J L Madara. Surface attachment of Salmonella typhimurium to intestinal epithelia imprints the subepithelial matrix with gradients chemotactic for neutrophils. *Journal of Cell Biology*, 131(6):1599–1608, December 1995.

[3] Nicholas Arpaia, Jernej Godec, Laura Lau, Kelsey E. Sivick, Laura M. McLaughlin, Marcus B. Jones, Tatiana Dracheva, Scott N. Peterson, Denise M. Monack, and Gregory M. Barton. TLR Signaling Is Required for Salmonella typhimurium Virulence. *Cell*, 144(5):675–688, March 2011.

[4] Andrea Haraga, Maikke B. Ohlson, and Samuel I. Miller. Salmonellae interplay with host cells. *Nature Reviews Microbiology*, 6(1):53–66, January 2008.

[5] M Martínez-Moya, M. A de Pedro, H Schwarz, and F García-del Portillo. Inhibition of Salmonella intracellular proliferation by non-phagocytic eucaryotic cells. *Research in Microbiology*, 149(5):309–318, May 1998.

[6] Hanna K. de Jong, Chris M. Parry, Tom van der Poll, and W. Joost Wiersinga. Host–Pathogen Interaction in Invasive Salmonellosis. *PLOS Pathogens*, 8(10):e1002933, October 2012.

[7] K. Z. Abshire and F. C. Neidhardt. Growth rate paradox of Salmonella typhimurium within host macrophages. *Journal of Bacteriology*, 175(12):3744–3748, June 1993.

[8] Daphne A. C. Stapels, Peter W. S. Hill, Alexander J. Westermann, Robert A. Fisher, Teresa L. Thurston, Antoine-Emmanuel Saliba, Isabelle Blommestein, Jörg Vogel, and Sophie Helaine. Salmonella persisters undermine host immune defenses during antibiotic treatment. *Science*, 362(6419):1156–1160, December 2018.

[9] John J. O'Shea and Peter J. Murray. Cytokine signaling modules in inflammatory responses. *Immunity*, 28(4):477–487, April 2008.

[10] David C. Dale, Laurence Boxer, and W. Conrad Liles. The phagocytes: Neutrophils and monocytes. *Blood*, 112(4):935–945, August 2008.

[11] Subhra K. Biswas and Eduardo Lopez-Collazo. Endotoxin tolerance: New mechanisms, molecules and clinical significance. *Trends in Immunology*, 30(10):475–487, October 2009.

[12] Sebastian E. Winter, Parameth Thiennimitr, Maria G. Winter, Brian P. Butler, Douglas L. Huseby, Robert W. Crawford, Joseph M. Russell, Charles L. Bevins, L. Garry Adams, Renée M. Tsolis, John R. Roth, and Andreas J. Bäumler. Gut inflammation provides a respiratory electron acceptor for Salmonella. *Nature*, 467(7314):426–429, September 2010.

[13] Sumati Murli, Robert O. Watson, and Jorge E. Galán. Role of tyrosine kinases and the tyrosine phosphatase SptP in the interaction of Salmonella with host cells. *Cellular Microbiology*, 3(12):795–810, 2001.

[14] Doris L. LaRock, Anu Chaudhary, and Samuel I. Miller. Salmonellae interactions with host processes. *Nature Reviews Microbiology*, 13(4):191–205, April 2015.

[15] Haihua Ruan, Zhen Zhang, Li Tian, Suying Wang, Shuangyan Hu, and Jian-Jun Qiao. The Salmonella effector SopB prevents ROS-induced apoptosis of epithelial cells by retarding TRAF6 recruitment to mitochondria. *Biochemical and Biophysical Research Communications*, 478(2):618–623, September 2016.

[16] Athma A. Pai, Golshid Baharian, Ariane Pagé Sabourin, Jessica F. Brinkworth, Yohann Nédélec, Joseph W. Foley, Jean-Christophe Grenier, Katherine J. Siddle, Anne Dumaine, Vania Yotova, Zachary P. Johnson, Robert E. Lanford, Christopher B. Burge, and Luis B. Barreiro. Widespread Shortening of 3' Untranslated Regions and Increased Exon Inclusion Are Evolutionarily Conserved Features of Innate Immune Responses to Infection. *PLOS Genetics*, 12(9):e1006338, September 2016.

[17] Marcelo B. Sztein, Andrea C. Bafford, and Rosângela Salerno-Goncalves. Salmonella enterica serovar Typhi exposure elicits ex vivo cell-type-specific epigenetic changes in human gut cells. *Scientific Reports*, 10(1):13581, August 2020.

[18] E. Lieberman-Aiden, N. L. van Berkum, L. Williams, M. Imakaev, T. Ragoczy, A. Telling, I. Amit, B. R. Lajoie, P. J. Sabo, M. O. Dorschner, R. Sandstrom, B. Bernstein, M. A. Bender, M. Groudine, A. Gnirke, J. Stamatoyannopoulos, L. A. Mirny, E. S. Lander, and J. Dekker. Comprehensive Mapping of Long-Range Interactions Reveals Folding Principles of the Human Genome. *Science*, 326(5950):289–293, October 2009.

[19] Elphège P. Nora, Bryan R. Lajoie, Edda G. Schulz, Luca Giorgetti, Ikuhiro Okamoto, Nicolas Servant, Tristan Piolot, Nynke L. van Berkum, Johannes Meisig, John Sedat, Joost Gribnau, Emmanuel Barillot, Nils Blüthgen, Job Dekker, and Edith Heard. Spatial partitioning of the regulatory landscape of the X-inactivation centre. *Nature*, 485(7398):381–385, May 2012.

[20] Diego Ottaviani, Elliott Lever, Shihong Mao, Rossitza Christova, Babatunji W. Ogunkolade, Tania A. Jones, Jaroslaw Szary, Johan Aarum, Muhammad A. Mumin, Christopher A. Pieri, Stephen A. Krawetz, and Denise Sheer. CTCF binds to sites in the major histocompatibility complex that are rapidly reconfigured in response to interferon-gamma. *Nucleic Acids Research*, 40(12):5262–5270, July 2012.

[21] Rossitza Christova, Tania Jones, Pei-Jun Wu, Andreas Bolzer, Ana P. Costa-Pereira, Diane Watling, Ian M. Kerr, and Denise Sheer. P-STAT1 mediates higher-order chromatin remodelling of the human MHC in response to IFNγ. *Journal of Cell Science*, 120(18):3262–3270, September 2007.

[22] Parimal Majumder, Jorge A. Gomez, Brian P. Chadwick, and Jeremy M. Boss. The insulator factor CTCF controls MHC class II gene expression and is required for the formation of long-distance chromatin interactions. *The Journal of Experimental Medicine*, 205(4):785–798, April 2008.

[23] Parimal Majumder and Jeremy M. Boss. Cohesin regulates major histocompatibility complex class II genes through interactions with MHC-II insulators. *Journal of immunology (Baltimore, Md. : 1950)*, 187(8):4236–4244, October 2011.

[24] Tatjana Nikolic, Dowty Movita, Margaretha EH Lambers, Claudia Ribeiro de Almeida, Paula Biesta, Kim Kreefft, Marjolein JW de Bruijn, Ingrid Bergen, Niels Galjart, Andre Boonstra, and Rudi Hendriks. The DNA-binding factor Ctcf critically controls gene expression in macrophages. *Cellular & Molecular Immunology*, 11(1):58–70, January 2014.

[25] Shutao Cai, Charles C. Lee, and Terumi Kohwi-Shigematsu. SATB1 packages densely looped, transcriptionally active chromatin for coordinated expression of cytokine genes. *Nature Genetics*, 38(11):1278–1288, November 2006.

[26] Mohamed El Gazzar, Barbara K. Yoza, Jean Y. Q. Hu, Sue L. Cousart, and Charles E. McCall. Epigenetic Silencing of Tumor Necrosis Factor α during Endotoxin Tolerance*. *Journal of Biological Chemistry*, 282(37):26857–26864, September 2007.

[27] Simmie L. Foster, Diana C. Hargreaves, and Ruslan Medzhitov. Gene-specific control of inflammation by TLR-induced chromatin modifications. *Nature*, 447(7147):972–978, June 2007.

[28] Hnin Thanda Aung, Kate Schroder, Stewart R. Himes, Kristian Brion, Wendy Van Zuylen, Angela Trieu, Harukazu Suzuki, Yoshihide Hayashizaki, David A. Hume, Matthew J. Sweet, and Timothy Ravasi. LPS regulates proinflammatory gene expression in macrophages by altering histone deacetylase expression. *The FASEB Journal*, 20(9):1315–1327, 2006.

[29] Jörg Mages, Harald Dietrich, and Roland Lang. A genome-wide analysis of LPS tolerance in macrophages. *Immunobiology*, 212(9-10):723–737, January 2008.

[30] Tao Yang, Feipeng Zhang, Galip Gürkan Yardımcı, Fan Song, Ross C Hardison, William Stafford, Feng Yue, and Qunhua Li. HiCRep: Assessing the reproducibility of Hi-C data using a stratum-adjusted correlation coefficient. page 37.

[31] John J. Seeley and Sankar Ghosh. Molecular mechanisms of innate memory and tolerance to LPS. *Journal of Leukocyte Biology*, 101(1):107–119, January 2017.

[32] Silvia Galan, Nick Machnik, Kai Kruse, Noelia Díaz, Marc A. Marti-Renom, and Juan M. Vaquerizas. CHESS enables quantitative comparison of chromatin contact data and automatic feature extraction. *Nature Genetics*, 52(11):1247–1255, November 2020.

[33] Uku Raudvere, Liis Kolberg, Ivan Kuzmin, Tambet Arak, Priit Adler, Hedi Peterson, and Jaak Vilo. G:profiler: A web server for functional enrichment analysis and conversions of gene lists (2019 update). *Nucleic Acids Research*, 47(W1):W191–W198, July 2019.

[34] Daniele Merico, Ruth Isserlin, Oliver Stueker, Andrew Emili, and Gary D. Bader. Enrichment Map: A Network-Based Method for Gene-Set Enrichment Visualization and Interpretation. *PLOS ONE*, 5(11):e13984, November 2010.

[35] Sergi Cuartero, Felix D. Weiss, Gopuraja Dharmalingam, Ya Guo, Elizabeth Ing-Simmons, Silvia Masella, Irene Robles-Rebollo, Xiaolin Xiao, Yi-Fang Wang, Iros Barozzi, Dounia Djeghloul, Mariane T. Amano, Henri Niskanen, Enrico Petretto, Robin D. Dowell, Kikuë Tachibana, Minna U. Kaikkonen, Kim A. Nasmyth, Boris Lenhard, Gioacchino Natoli, Amanda G. Fisher, and Matthias Merkenschlager. Control of inducible gene expression links cohesin to hematopoietic progenitor self-renewal and differentiation. *Nature Immunology*, 19(9):932–941, September 2018.

[36] Grégoire Stik, Enrique Vidal, Mercedes Barrero, Sergi Cuartero, Maria Vila-Casadesús, Julen Mendieta-Esteban, Tian V. Tian, Jinmi Choi, Clara Berenguer, Amaya Abad, Beatrice Borsari, François le Dily, Patrick Cramer, Marc A. Marti-Renom, Ralph Stadhouders, and Thomas Graf. CTCF is dispensable for immune cell transdifferentiation but facilitates an acute inflammatory response. *Nature Genetics*, 52(7):655–661, July 2020.

[37] Laurel E. Hind, Emily B. Lurier, Micah Dembo, Kara L. Spiller, and Daniel A. Hammer. Effect of M1–M2 Polarization on the Motility and Traction Stresses of Primary Human Macrophages. *Cellular and Molecular Bioengineering*, 9(3):455–465, September 2016.

[38] E.V. Volpi, E. Chevret, T. Jones, R. Vatcheva, J. Williamson, S. Beck, R.D. Campbell, M. Goldsworthy, S.H. Powis, J. Ragoussis, J. Trowsdale, and D. Sheer. Large-scale chromatin organization of the major histocompatibility complex and other regions of human chromosome 6 and its response to interferon in interphase nuclei. *Journal of Cell Science*, 113(9):1565–1576, May 2000.

[39] Katharine J. Goodall, Angela Nguyen, Lucy C. Sullivan, and Daniel M. Andrews. The expanding role of murine class Ib MHC in the development and activation of Natural Killer cells. *Molecular Immunology*, 115:31–38, November 2019.

[40] M. Ryan Corces, Alexandro E. Trevino, Emily G. Hamilton, Peyton G. Greenside, Nicholas A. Sinnott-Armstrong, Sam Vesuna, Ansuman T. Satpathy, Adam J. Rubin, Kathleen S. Montine, Beijing Wu, Arwa Kathiria, Seung Woo Cho, Maxwell R. Mumbach, Ava C. Carter, Maya Kasowski, Lisa A. Orloff, Viviana I. Risca, Anshul Kundaje, Paul A. Khavari, Thomas J. Montine, William J. Greenleaf, and Howard Y. Chang. An improved ATAC-seq protocol reduces background and enables interrogation of frozen tissues. *Nature Methods*, 14(10):959–962, October 2017.

[41] Rita Figueira, Kathryn G. Watson, David W. Holden, and Sophie Helaine. Identification of Salmonella Pathogenicity Island-2 Type III Secretion System Effectors Involved in Intramacrophage Replication of S. enterica Serovar Typhimurium: Implications for Rational Vaccine Design. *mBio*, 4(2):e00065–13.

[42] Cyril Matthey-Doret, Lyam Baudry, Amaury Bignaud, Axel Cournac, Remi Montagne, Nadège Guiglielmoni, Foutel-Rodier Théo, and Scolari Vittore F. Simple library/pipeline to generate and handle Hi-C data. https://github.com/koszullab/hicstuff, March 2021.

[43] Nezar Abdennur and Leonid A Mirny. Cooler: Scalable storage for Hi-C data and other genomically labeled arrays. *Bioinformatics*, 36(1):311–316, January 2020.

[44] Open2c/cooltools. Open Chromosome Collective, April 2021.

[45] Cyril Matthey-Doret, Lyam Baudry, Axel Breuer, Rémi Montagne, Nadège Guiglielmoni, Vittore Scolari, Etienne Jean, Arnaud Campeas, Philippe Henri Chanut, Edgar Oriol, Adrien Méot, Laurent Politis, Antoine Vigouroux, Pierrick Moreau, Romain Koszul, and Axel Cournac. Computer vision for pattern detection in chromosome contact maps. *Nature Communications*, 11(1):5795, November 2020.

[46] Cyril Matthey-Doret. Koszullab/pareidolia: V0.6.1. https://zenodo.org/record/5062485, July 2021.

[47] Zhuoqing Fang. Gseapy: Gene Set Enrichment Analysis in Python.

[48] Aaron R. Quinlan and Ira M. Hall. BEDTools: A flexible suite of utilities for comparing genomic features. *Bioinformatics*, 26(6):841–842, March 2010.

Supplementary figures

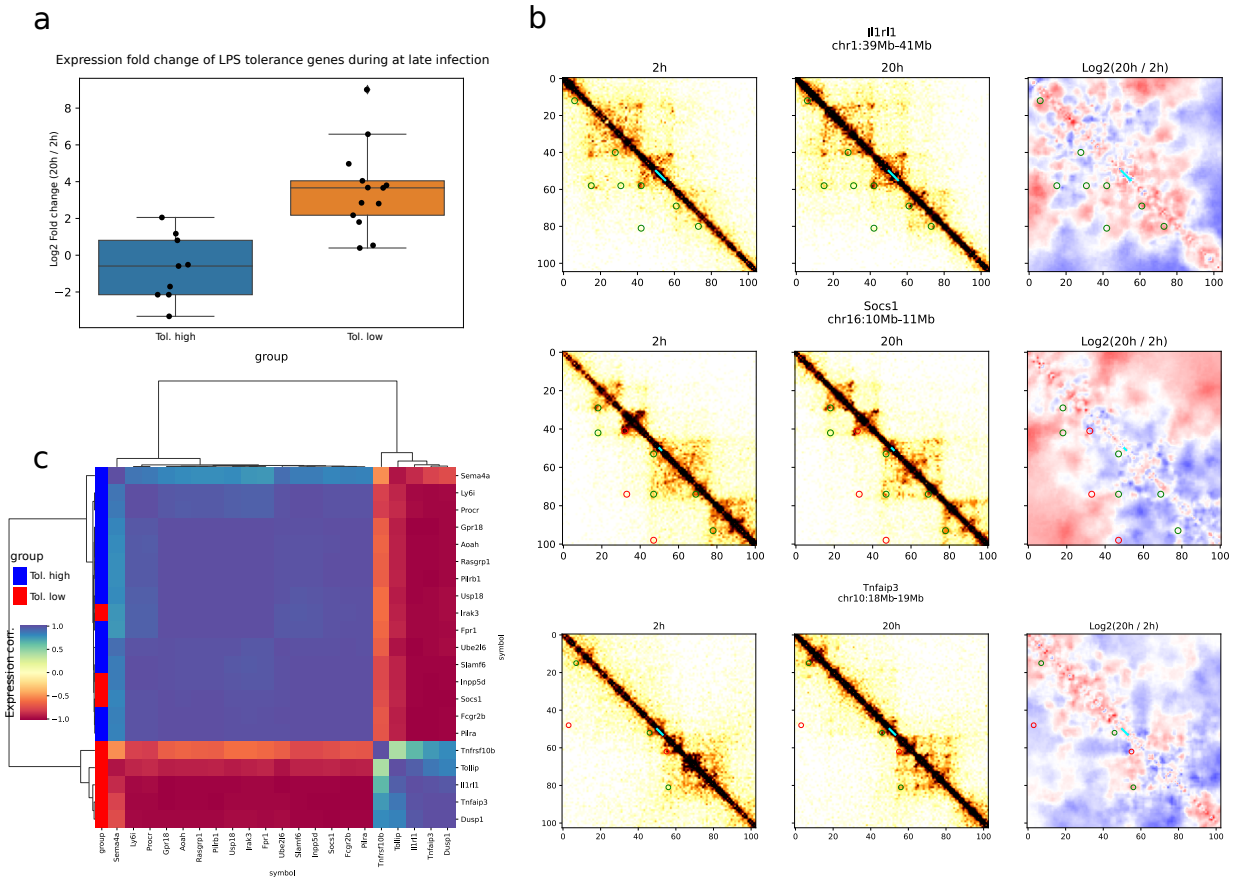

Figure S1: Analysis of select LPS response marker genes from [29]. **a,** Expression of 22 genes known to be positive (Tol. up) or negative (Tol. low) regulators of the LPS response, in our RNAseq results. **b,** Example Hi-C regions from genes with strong loop changes. Contacts at early (2h, left) late (20h, middle) and change during late infection (20h/2h, right) are shown. All matrices were binned at 10kb and ratios are smoothed using Serpentine adaptive binning. **c,** Gene expression correlation between LPS marker genes. Pearson correlation across all 4 samples is shown (duplicates at 2h and 20h).

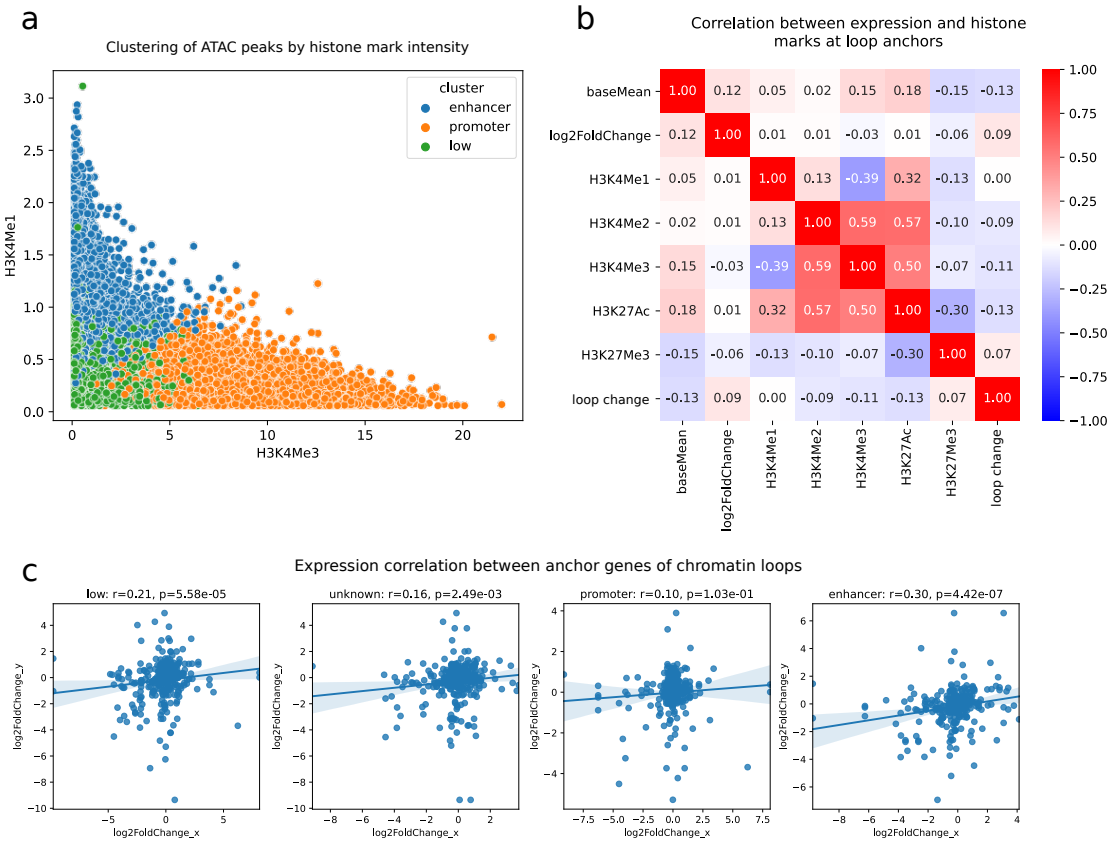

Figure S2: Analysis of epigenetic marks at loop anchors. **a,** Distribution of ATACseq peaks based on histone mark intensities H3K4Me3 and H3K4Me1. Colors represent cluster value assigned on the basis of 5 histone marks (H3K4Me1, H3K4Me2, H3K4Me3, H3K27Ac, H3K27Me3). **b,** Correlation between base gene expression (baseMean), gene expression fold change during infection (log2FoldChange), histone marks and loop intensity change during infection (loop change) at loop anchors. **c,** Expression correlation between gene pairs at loop anchors based on loop categories. Loop categories are defined as either anchor containing a histone mark-derived annotation.

Table S1: Table of significantly enriched GO terms for genes in CHESS-detected regions with structural changes.

source	name	id	logqval	size	intersect
GO:MF	protein binding	GO:0005515	9.089	10189	534
GO:MF	binding	GO:0005488	7.078	14895	712
GO:MF	TAP binding	GO:0046977	5.547	12	8
GO:MF	TAP complex binding	GO:0062061	5.276	9	7
GO:MF	enzyme binding	GO:0019899	4.827	2164	144
GO:MF	identical protein binding	GO:0042802	4.644	2140	142
GO:MF	CD8 receptor binding	GO:0042610	4.346	11	7
GO:MF	transcription factor binding	GO:0008134	4.272	571	53
GO:MF	protein-containing complex binding	GO:0044877	4.083	1464	104
GO:MF	beta-2-microglobulin binding	GO:0030881	3.982	12	7
GO:MF	ion binding	GO:0043167	3.421	5862	314
GO:MF	anion binding	GO:0043168	3.026	2420	149
GO:MF	transferase activity	GO:0016740	2.852	2277	141
GO:MF	T cell receptor binding	GO:0042608	2.673	17	7
GO:MF	oligopeptide binding	GO:1900750	2.673	17	7
GO:MF	glutathione binding	GO:0043295	2.673	17	7
GO:MF	organic cyclic compound binding	GO:0097159	2.382	5768	303

source	name	id	logqval	size	intersect
GO:MF	glutathione transferase activity	GO:0004364	2.366	33	9
GO:MF	catalytic activity	GO:0003824	2.332	5665	298
GO:MF	peptide antigen binding	GO:0042605	2.292	19	7
GO:MF	heterocyclic compound binding	GO:1901363	2.286	5672	298
GO:MF	transcription coregulator activity	GO:0003712	2.273	448	40
GO:MF	protein homodimerization activity	GO:0042803	2.063	676	53
GO:MF	protein dimerization activity	GO:0046983	1.809	1052	73
GO:BP	metabolic process	GO:0008152	12.491	11429	598
GO:BP	cellular metabolic process	GO:0044237	12.464	10350	554
GO:BP	organic substance metabolic process	GO:0071704	11.676	10989	577
GO:BP	primary metabolic process	GO:0044238	10.626	10243	542
GO:BP	cellular nitrogen compound metabolic process	GO:0034641	10.222	6201	364
GO:BP	nitrogen compound metabolic process	GO:0006807	9.931	9669	515
GO:BP	macromolecule metabolic process	GO:0043170	8.141	9484	499
GO:BP	biosynthetic process	GO:0009058	7.867	5882	339
GO:BP	cellular macromolecule metabolic process	GO:0044260	7.821	7962	432
GO:BP	cellular biosynthetic process	GO:0044249	7.801	5715	331
GO:BP	organic cyclic compound metabolic process	GO:1901360	7.314	5829	334
GO:BP	cellular aromatic compound metabolic process	GO:0006725	7.256	5618	324
GO:BP	organic substance biosynthetic process	GO:1901576	7.165	5779	331
GO:BP	nucleobase-containing compound metabolic process	GO:0006139	6.484	5416	311
GO:BP	cellular response to stress	GO:0033554	6.394	1805	132
GO:BP	heterocycle metabolic process	GO:0046483	6.381	5535	316
GO:BP	cellular macromolecule biosynthetic process	GO:0034645	6.147	4744	278
GO:BP	regulation of cellular biosynthetic process	GO:0031326	5.978	4088	246
GO:BP	cellular nitrogen compound biosynthetic process	GO:0044271	5.903	4705	275
GO:BP	macromolecule biosynthetic process	GO:0009059	5.773	4782	278
GO:BP	regulation of biosynthetic process	GO:0009889	5.593	4167	248
GO:BP	nucleic acid metabolic process	GO:0090304	5.483	4962	285
GO:BP	protein localization	GO:0008104	5.040	2452	161
GO:BP	regulation of cellular macromolecule biosynthetic process	GO:2000112	4.908	3880	231
GO:BP	organonitrogen compound metabolic process	GO:1901564	4.822	6326	344
GO:BP	aromatic compound biosynthetic process	GO:0019438	4.752	4042	238
GO:BP	nucleobase-containing compound biosynthetic process	GO:0034654	4.706	3963	234
GO:BP	heterocycle biosynthetic process	GO:0018130	4.684	4028	237
GO:BP	organic cyclic compound biosynthetic process	GO:1901362	4.628	4181	244
GO:BP	regulation of macromolecule biosynthetic process	GO:0010556	4.581	3913	231
GO:BP	RNA metabolic process	GO:0016070	4.305	4470	256
GO:BP	transcription DNA-templated	GO:0006351	4.236	887	211
GO:BP	nucleic acid-templated transcription	GO:0097659	4.217	3534	211
GO:BP	RNA biosynthetic process	GO:0032774	4.068	3549	211
GO:BP	gene expression	GO:0010467	4.055	5933	322
GO:BP	cellular protein metabolic process	GO:0044267	3.910	4815	270
GO:BP	regulation of transcription DNA-templated	GO:0006355	3.796	887	203
GO:BP	regulation of nucleic acid-templated transcription	GO:1903506	3.777	3413	203
GO:BP	regulation of RNA biosynthetic process	GO:2001141	3.738	3417	203
GO:BP	protein metabolic process	GO:0019538	3.677	5474	299
GO:BP	regulation of nitrogen compound metabolic process	GO:0051171	3.582	5706	309
GO:BP	cellular macromolecule localization	GO:0070727	3.453	1726	117
GO:BP	localization	GO:0051179	3.440	6168	329
GO:BP	macromolecule localization	GO:0033036	3.393	2897	176
GO:BP	cellular protein localization	GO:0034613	3.360	1714	116
GO:BP	regulation of cellular metabolic process	GO:0031323	3.318	6073	324
GO:BP	regulation of primary metabolic process	GO:0080090	3.221	5886	315
GO:BP	cellular localization	GO:0051641	3.164	2777	169
GO:BP	nitrogen compound transport	GO:0071705	3.094	1986	129
GO:BP	regulation of nucleobase-containing compound metabolic process	GO:0019219	3.059	3931	224
GO:BP	regulation of RNA metabolic process	GO:0051252	2.941	3691	212

source	name	id	logqval	size	intersect
GO:BP	regulation of macromolecule metabolic process	GO:0060255	2.835	6363	334
GO:BP	positive regulation of cellular biosynthetic process	GO:0031328	2.755	1956	126
GO:BP	establishment of localization	GO:0051234	2.720	4658	256
GO:BP	positive regulation of nitrogen compound metabolic process	GO:0051173	2.714	3069	181
GO:BP	positive regulation of nucleic acid-templated transcription	GO:1903508	2.650	1616	108
GO:BP	regulation of metabolic process	GO:0019222	2.646	6841	354
GO:BP	positive regulation of RNA biosynthetic process	GO:1902680	2.637	1617	108
GO:BP	establishment of protein localization	GO:0045184	2.502	1647	109
GO:BP	macromolecule modification	GO:0043412	2.358	3823	215
GO:BP	positive regulation of biosynthetic process	GO:0009891	2.268	1999	126
GO:BP	positive regulation of macromolecule metabolic process	GO:0010604	2.149	3467	197
GO:BP	nitrobenzene metabolic process	GO:0018916	2.111	4	4
GO:BP	cellular component organization or biogenesis	GO:0071840	2.090	6270	325
GO:BP	positive regulation of metabolic process	GO:0009893	2.007	3760	210
GO:BP	localization within membrane	GO:0051668	2.003	654	53
GO:BP	protein transport	GO:0015031	1.984	1535	101
GO:BP	regulation of gene expression	GO:0010468	1.978	4888	262
GO:BP	protein localization to membrane	GO:0072657	1.948	589	49
GO:BP	transport	GO:0006810	1.929	4502	244
GO:BP	positive regulation of nucleobase-containing compound metabolic process	GO:0045935	1.920	1912	120
GO:BP	organic substance transport	GO:0071702	1.903	2416	145
GO:BP	positive regulation of cellular metabolic process	GO:0031325	1.817	3275	186
GO:BP	positive regulation of RNA metabolic process	GO:0051254	1.804	1745	111
GO:BP	positive regulation of macromolecule biosynthetic process	GO:0010557	1.799	1844	116
GO:BP	transcription by RNA polymerase II	GO:0006366	1.762	2492	148
GO:BP	cellular protein modification process	GO:0006464	1.745	3644	203
GO:BP	protein modification process	GO:0036211	1.745	3644	203
GO:BP	cellular response to organic substance	GO:0071310	1.744	2453	146
GO:BP	cellular response to chemical stimulus	GO:0070887	1.725	3097	177
GO:BP	cellular component organization	GO:0016043	1.655	6090	314
GO:BP	positive regulation of protein-containing complex assembly	GO:0031334	1.598	240	26
GO:BP	antigen processing and presentation of peptide antigen	GO:0048002	1.513	64	12
GO:BP	establishment of localization in cell	GO:0051649	1.512	2031	124
GO:BP	cellular response to organic cyclic compound	GO:0071407	1.497	595	48
GO:BP	response to stress	GO:0006950	1.404	3817	209
GO:BP	negative regulation of cellular process	GO:0048523	1.348	5068	266
GO:BP	xenobiotic catabolic process	GO:0042178	1.312	15	6
GO:CC	intracellular anatomical structure	GO:0005622	29.657	14111	750
GO:CC	membrane-bounded organelle	GO:0043227	24.868	11812	654
GO:CC	organelle	GO:0043226	23.998	12827	690
GO:CC	intracellular membrane-bounded organelle	GO:0043231	22.652	11363	630
GO:CC	intracellular organelle	GO:0043229	22.543	12510	674
GO:CC	cytoplasm	GO:0005737	19.392	11093	609
GO:CC	intracellular organelle lumen	GO:0070013	12.853	4581	296
GO:CC	organelle lumen	GO:0043233	12.840	4582	296
GO:CC	membrane-enclosed lumen	GO:0031974	12.840	4582	296
GO:CC	nucleus	GO:0005634	9.341	7208	404
GO:CC	nuclear lumen	GO:0031981	9.119	4062	256
GO:CC	nucleoplasm	GO:0005654	8.838	3560	230
GO:CC	cytosol	GO:0005829	7.797	3849	240
GO:CC	intracellular protein-containing complex	GO:0140535	5.380	712	64
GO:CC	protein-containing complex	GO:0032991	5.201	5312	297
GO:CC	bounding membrane of organelle	GO:0098588	4.812	1676	117
GO:CC	MHC class I peptide loading complex	GO:0042824	4.727	15	8
GO:CC	MHC class I protein complex	GO:0042612	4.590	11	7
GO:CC	endomembrane system	GO:0012505	4.303	4006	231
GO:CC	mitochondrion	GO:0005739	4.303	1827	123
GO:CC	organelle membrane	GO:0031090	4.074	3076	185

source	name	id	logqval	size	intersect
GO:CC	endoplasmic reticulum exit site	GO:0070971	3.882	31	10
GO:CC	nuclear protein-containing complex	GO:0140513	3.060	1168	83
GO:CC	intracellular non-membrane-bounded organelle	GO:0043232	3.041	4500	247
GO:CC	non-membrane-bounded organelle	GO:0043228	2.928	4515	247
GO:CC	Golgi medial cisterna	GO:0005797	2.817	24	8
GO:CC	Golgi apparatus	GO:0005794	2.804	1449	97
GO:CC	endoplasmic reticulum	GO:0005783	2.761	1761	113
GO:CC	endoplasmic reticulum protein-containing complex	GO:0140534	2.220	135	18
GO:CC	endoplasmic reticulum membrane	GO:0005789	2.138	993	70
GO:CC	catalytic complex	GO:1902494	2.103	1334	88
GO:CC	endoplasmic reticulum subcompartment	GO:0098827	2.054	999	70
GO:CC	nuclear outer membrane-endoplasmic reticulum membrane network	GO:0042175	2.047	1018	71
GO:CC	COPII-coated ER to Golgi transport vesicle	GO:0030134	1.990	58	11
GO:CC	MHC protein complex	GO:0042611	1.912	23	7
GO:CC	perinuclear region of cytoplasm	GO:0048471	1.846	776	57
GO:CC	organelle subcompartment	GO:0031984	1.737	1580	99
GO:CC	intercellular bridge	GO:0045171	1.470	77	12
GO:CC	intrinsic component of endoplasmic reticulum membrane	GO:0031227	1.451	154	18
GO:CC	mitochondrial outer membrane	GO:0005741	1.354	185	20
GO:CC	cytoplasmic vesicle membrane	GO:0030659	1.346	489	39